

Substorms, Pseudobreakups and Quiescent Events Caused by Interplanetary Shocks

Xiaoyan Zhou and Bruce T. Tsurutani

Jet Propulsion Laboratory, California Institute of Technology,
Pasadena, California

Abstract

We use WIND solar wind data and POLAR UV imaging data to study magnetospheric responses and substorm triggering mechanisms during and after interplanetary (IP) shock events. Of 53 IP shock events that occurred in 1997 and 1998 at WIND, 18 events have POLAR near-midnight UV images available. All of these 18 events are used in this study. The nightside auroral responses are classified into three types: substorm expansion phase (SS) (or substorm further intensification) events, pseudobreakup (PB) events, and quiescent (QE) events. It is found that the solar wind precondition determines the causes of the different auroral responses, with a ~ 1.5 hr “precondition” (upstream of the IP shock) giving the best empirical results. The upstream IMF B_z is strongly southward prior to substorm triggerings (44% of all events), the IMF B_z is ~ 0 nT for PB triggerings (39% of all events), and the IMF is almost purely northward for quiescent events (17%). A magnetotail-compression substorm triggering model is developed and presented. This model uses dayside magnetic reconnection to load the near-Earth plasma sheet and a current disruption mechanism to unload the stored energy. We call this model a Dripping, Tilting Bucket (DTB) model.

1. Introduction

Numerous works (Heppner, 1955; Schieldge and Siscoe, 1970; Kawasaki et al., 1971; Burch, 1972; Kokubun et al., 1977; and Akasofu and Chao, 1980) have demonstrated that magnetospheric substorm expansion phases can be triggered by interplanetary (IP) shocks (although most of these earlier studies used Storm Sudden Commencements (SSCs) in their analyses rather than shocks, it is now believed that these are essentially equivalent). Schieldge and Siscoe (1970), Kawasaki et al. (1971) and Kokubun et al. (1977) concluded that substorm triggerings are more probable following more intense SSCs. Interplanetary and magnetospheric preconditions also appear to be important factors. Burch (1972) and Kokubun et al. (1977) noted a higher probability of triggering if there were southward interplanetary magnetic fields (IMF) 30 min prior to the SSCs. Schieldge and Siscoe (1970) found that substorm triggerings were more probable when the low latitude magnetic H component in the premidnight sector was depressed. Specifically, Kokubun et al. (1977) noted that “Negative bays at auroral latitudes followed 43% of the SSC and SI (sudden impulse) events examined. In approximately 90% of these cases, the AE indices showed appreciable activity ($AE > 100$ nT) during an interval of 15 min before the SSC.”

While the above works showed that substorm triggering by interplanetary shocks occurs ~ 43% of the time (Kokubun et al., 1977), what they did not address is “what happens during other 57% of the time when substorms do not occur?” Another fundamental question is what is the physical mechanism for substorm triggering/lack of triggering and how does this fit into present day nonshock substorm scenarios?

The purpose of this paper is to use WIND interplanetary data and POLAR UV imaging data to determine the nightside auroral zone effects when IP shocks compress the

magnetosphere/magnetotail. All of the IP shock events for 1997 and 1998 have been surveyed. We will specifically focus on events where clear imaging of the entire nightside auroral zone is available. Thus any possible faint auroral substorm activity will be detected (this technique is superior to the use of AE; the indices are often composed of only 12 ground stations, and small auroral events may be missed). We will show that during some shock events, small localized brightenings occur near midnight. They are of low intensity and have rapid fadings. We have identified these as pseudobreakup (PB) events. Finally we will develop a shock compression model that will explain why and when substorm triggerings will or will not occur. This model can be easily extended to be applicable to non-shock triggered substorms.

2. Events and Data Set

A data set of 27 interplanetary shocks/pressure pulses in 1997 and 26 events in 1998 (a total of 53 events) has been identified by the WIND magnetometer team (R.P. Lepping, private communication, 1999). Of these 53 events, there are 18 where the UV images are useful for this study. For the other events, POLAR was at locations where the nightside aurora could not be imaged. Dayside auroral images, when available, are used to identify and verify the shock arrival time at the magnetopause nose (by the associated dayside auroral brightening; Zhou and Tsurutani, 1999). Nightside auroral images are used in this study to identify whether substorms or PB events or nothing are triggered by IP shocks.

The solar wind plasma and interplanetary magnetic field (IMF) data are obtained from the WIND SEW (the Solar Wind Experiment) and MFI (the Magnetic Field Investigation) experiments. These experiments are described in Ogilvie et al. (1995) and Lepping et al. (1995), respectively. The time resolution used in this study are ~ 46 sec for the MFI and 1.5 min for SEW. The auroral imaging data used in this investigation are taken by the

Ultraviolet Imager (UVI) on board the POLAR earth-orbiting satellite. The satellite has an apogee of $\sim 9 R_E$ located over the north pole. The camera has four filters, two of which are primarily used in this study. They are the Lyman-Birge-Hopfield (LBH) short wavelength filter centered at $\sim 1500 \text{ \AA}$ and the LBH long wavelength filter at $\sim 1700 \text{ \AA}$ (for molecular nitrogen lines). The angular resolution is 0.04° per pixel, and the CCD is a 224 by 200 pixel array (Torr et al., 1995). The cadence is 37 s when the LBH long filter is used alone (3 events) and 1 min 50 s when both the long and short filters are used (12 events). For the remaining three events the cadence is 6 min 8 s.

Table 1. IP shock-POLAR UVI events.

Event date	IS at WIND (UT)	IS at Earth (UT)
Jan 10, 1997	0052	0103
Aug 9, 1997	0610	0641
Sep 18, 1997	0031	0059
Oct 1, 1997	0057	0100
Oct 10, 1997	1600	1616
Oct 23, 1997	0810	0808
Nov 1, 1997	0614	0636
Nov 22, 1997	0910	0950
Dec 10, 1997	0430	0525
Apr 7, 1998	1655	1804
May 3, 1998	1700	1745
May 29, 1998	1510	1539
Jun 13, 1998	1920	2001
Jun 25, 1998	1610	1624
Aug 10, 1998	0030	0045
Sep 8, 1998	1707	1753
Sep 24, 1998	2320	2348
Oct 2, 1998	0700	0724

The 18 IP shock-related auroral events used in this study are listed in Table 1. Column 1 are the event dates listed in chronological order. Column 2 are the time that the IP shocks detected at WIND. Column 3 are the IP shock arrival times at the nose of the magnetopause. The latter are calculated based on the IP shock speeds and the distance between WIND and the magnetopause (the nose is assumed to be located at $X = 10 R_E$). The calculated IP shock arrival times have been double-checked with dayside auroral

brightening onsets described above (Zhou and Tsurutani, 1999). The timings are found to be in agreement within 1-3 min.

In the study, we examine different interplanetary average parameters upstream of the IP shocks to examine the “interplanetary preconditions”. Among them, B is IMF $|B|$, B_s is the southward component of the IMF B_z (i.e. $B_s=|B_z|$, when $B_z<0$; and $B_s=0$, when $B_z\geq 0$), B_n is the northward IMF B_z component (i.e. $B_n=B_z$, when $B_z>0$; and $B_n=0$, when $B_z\leq 0$), and ram pressure, defined as $P_{ram}=1.16\rho_p V_{sw}^2$ where we assume a value for $N_{He^{++}}=4\%N_{H^+}$ (the helium data is unfortunately not available). In the above, ρ_p is the mass density of protons, and V_{sw} is the solar wind velocity. The solar wind static pressure is the summation of the magnetic and plasma thermal pressures, $P_{st}=B^2/8\pi+(n_p kT_p+n_e kT_e)$, where n_p and n_e are the number density of protons and electrons, k is Boltzmann’s constant, T_p and T_e are the proton (ion) and electron temperatures. ΔP_{ram} and ΔP_{st} are the increases in solar wind ram and static pressures across the IP (forward) shocks, respectively.

Ground base indices will also be examined. The average AL indices prior to the IP shock arrivals (at the magnetopause) are used as indicators of ionospheric preconditions. Peak AL values from the shock arrival times to half hour after the shocks are used to determine the “magnetospheric responses”. This data is complementary to the UV images.

For the solar wind upstream of the IP shocks, intervals up to 3.0 hr were examined. We find that the interval of 1.5 hr gave the best fits to the concomitant geomagnetic activity (not shown), and we only discuss the latter results here.

3. Case Studies

3.1 The Substorm event of September 24, 1998

On September 24, 1998, there was a significant ISTP-SEC event initiated by a M6.9 solar flare. There was an extremely intense series of type III radio bursts and type III storms. An interplanetary shock and associated fast interplanetary coronal mass ejection (ICME) were detected by the WIND spacecraft, at X=185 Re upstream of the Earth.

The solar wind conditions observed by WIND plus the corresponding ground based AE and AL indices are shown in Figure 1. The IP shock is denoted by a vertical dashed line at 2320 UT in the top panel. Prior to the IP shock, the IMF magnitude was high (~ 12 nT), and the IMF B_z was \sim zero 40 min prior to the shock. However, B_z was ~ -10 nT in previous 3 hours (not all shown). The solar wind plasma preconditions are: the plasma density is ~ 10 cm⁻³, the solar wind speed is $\sim 425 - 450$ km/s and therefore the calculated ram pressure is ~ 4 nPa. There was substorm activity prior to the IP shock arrival (which is presumably associated with the long duration southward IMF B_z , especially from ~ 1920 UT to ~ 2210 UT). At the IP shock, the IMF magnitude increased to ~ 40 nT, the ram pressure increased by a factor of 4 and static pressure by 10. The above interplanetary pressure enhancements are the largest of the 18 events studied. The shock arrived at the Earth's dayside magnetopause at ~ 2345 UT (the dashed line in the lower panel). Immediately after the shock, AL decreased from ~ -500 to ~ -1600 nT (AE increased from ~ 650 to ~ 2000 nT).

The solar wind static pressure is typically lower than the solar wind ram pressure by about two orders of magnitude (see Figure 1 and above comments). Thus magnetosphere/magnetotail compression is primarily caused by the solar wind ram pressure. However, in the near-Earth tail, where the flaring angle is small, the contribution

of the solar wind static pressure can be important. For the Sep 24, 1998 event, the static pressure contributes ~ 0.25 of the total solar wind compression at $X = -15$ Re. The method of calculation and details will be discussed later in Section 5.

The shock arrival at Earth occurred at ~ 2345 UT and is associated with the near-noon auroral brightening shown in panel (c), Plate 1. Such noon auroral brightenings and expansion (when data available) are noted for all of the 18 events studied. The physical mechanisms for shock-auroral brightenings and longitudinal expansions are beyond the scope of the present paper but are discussed in Zhou and Tsurutani (1999) and Tsurutani et al. (1999) for the interested reader.

Before the IP shock arrival, there was substorm activity at ~ 21 MLT as shown by Plate 1 panels (a) and (b). The auroral activity is consistent with the high AL values (400 to 600 nT) shown previously in Figure 1. About 4 minutes after the IP shock arrival (2348 UT), the peak of the substorm auroral illumination at ~ 21 MLT increases from ~ 100 photons $\text{cm}^{-2} \text{s}^{-1}$ (at ~ 2344 UT) to over 400 photons $\text{cm}^{-2} \text{s}^{-1}$ (at ~ 2348 UT, Plate 1, panel f). The area of auroral brightness also expands to a region covering $\sim 8^\circ$ latitude by 18° longitude. The corresponding AL intensification is from ~ 560 nT to ~ 1700 nT (AE increases from ~ 730 nT to ~ 2000 nT). New auroral forms in the local time sector between 21 to 3 MLT also develop and evolve within minutes after the shock arrival at the magnetopause. Auroral forms expand poleward to approach 73° magnetic latitude by 2351 UT (panel i), and reach 80° by 0005 UT, Sep 25 (not shown). It is clear that more is happening than a simple “substorm intensification”. However, detailed analyses of this complex event is beyond the scope of this present study, and will be addressed in a later work.

3.2 The PB event of August 9, 1997

Figure 2 gives an example of an interplanetary “pressure wave” on August 9, 1997. Although this “pressure wave” was not found to be a shock (D. Berdichevsky and Y. Whang, private communication, 1999), there are a significant ram and static pressure increases occurring across the event (in the model that we will present in a later section, it will be assumed that there is little difference between a pressure wave and a shock for triggering substorms). In the top panel, the vertical dashed line at ~ 0610 UT denotes the beginning of the pressure ramp where the thermal velocity abruptly increases and the IMF B_z turns southward, decreasing from 0 to -3 nT. Prior to the pressure ramp, the magnetic field magnitude is low (~ 4 nT), the plasma density is high (~ 15 cm $^{-3}$), and the solar wind speed is low (~ 335 km/s). The IMF B_z is near zero with a small average value of ~ 0.3 nT (1.5 hr average) and a sporadic southward component. Across the pressure ramp, the solar wind speed increases slightly from ~ 340 km/s to ~ 360 km/s and the density increases from ~ 18 cm $^{-3}$ to a downstream maximum of ~ 26 cm $^{-3}$. The calculated ram pressure increases from 3.8 nPa to a maximum downstream value of 6.0 nPa.

The high plasma density and low speed of the solar wind prior to the pressure pulse indicate that this region is most probably a heliospheric current sheet (HCS) plasma sheet (Winterhalter et al., 1994). There is no shock for this event, only a pressure increase due to the monotonic rise in both solar wind speed and density. Low geomagnetic activity prior to and during HCS plasma sheet encounters have been previously noted by Tsurutani et al. (1995).

As shown at the bottom panel of Figure 2, the auroral zone was very quiet, AL ~ 0 nT (AE ~ 40 nT) during the 3 hr interval prior to the pressure wave arrival at Earth. Approximately, ~ 12 min after the IP shock arrival at the magnetopause, a small magnetic disturbance is

measured in AL (and AE). The AL value increases from ~ 0 to a maximum of ~ 35 nT (AE to ~ 90 nT) at ~ 0700 UT. This small enhancement is a pseudobreakup. A half hour later (~ 0730 UT), there was a substorm expansion phase with an AL value ~ 200 nT (and AE ~ 300 nT).

Figure 3 shows that from $\sim 0652 - 0730$ UT, very localized and weak geomagnetic disturbances were measured by the CANOPUS ground based magnetometers. Panel (a) gives a map of CANOPUS ground station locations. Circles are drawn at the stations where the small (PB) negative bays were detected. Panel (b) gives the magnetic X-component variations along a meridional chain (at $\sim 265^\circ$ geographic longitude). The first weak magnetic bay is detected only at Gillam (GILL) in this chain and is denoted by the vertical dashed line at ~ 0652 UT. During the recovery of this small bay, there is another small disturbance (small bay?) occurring at ~ 0714 UT (the second vertical dashed line). Panel (c) gives the magnetogram X-components of the east-west CANOPUS stations. The disturbances are detected by Rabbit Lake (RABB), and at Fort Smith (FSMI) (where the effect is much weaker). The two small magnetic bay onsets are detected simultaneously at GILL, RABB and FSMI. The maximum amplitude of the first bay is ~ 140 nT (at GILL RABB) and ~ 100 nT for the second event (also at GILL and RABB).

Plate 2 gives a sequence of POLAR UV images for this event. The UV images are presented in geographic coordinates with an underlying northern hemisphere map. Geomagnetic local noon is at the top left and midnight is at the bottom right. Note that this area is over Canada. Panel (a) (upper left) is the north polar region prior to the pressure pulse arrival. Panel (b) at 0643:59 UT shows an enhanced brightening (red area) centered at 1430 MLT, indicating the effects of the arrival of the interplanetary pressure pulse.

At the time of the first small negative bay of Figure 3 (0625 UT), there is a nightside auroral brightening to ~ 20 photons $\text{cm}^{-2} \text{s}^{-1}$ (panel e, 0653:11 UT). The intensity of the aurora in the previous image taken ~ 3 min earlier (panel b) is only ~ 10 photons $\text{cm}^{-2} \text{s}^{-1}$. Panel (f), at a later time of 0656:15 UT, shows a clear, near-midnight, bright auroral spot (~ 40 photons $\text{cm}^{-2} \text{s}^{-1}$). The delay time from the pressure pulse arrival at the magnetopause to panel (f) is ~ 12 min. The center of the spot is located at 67° geomagnetic latitude and 2310 MLT. In geographic coordinates, the location of the red area (auroral intensities of 40 to 45 photons $\text{cm}^{-2} \text{s}^{-1}$) is 55° to 58° in latitude, and 255° to 261° in longitude. The size of the red auroral spot is thus $\sim 3^\circ \times 6^\circ$, consistent with the CANOPUS ground magnetometer responses. Panels (g), (h) and (i) show that this auroral spot fades within ~ 10 min. The peak brightening time of 0702:23 UT (Panel h) is near the peak amplitude of the first small magnetic bay shown in Figure 3.

At 0714:39 UT another local midnight auroral spot brightens at the same location (Plate 2, panel l). This occurs at the time of the onset of the second small magnetic bay of Figure 3. This second spot peaks in intensity at 0717:43 UT. The size of the red area is $\sim 3^\circ \times 8^\circ$ (panel m) and it decays within ~ 10 min. This gives a ~ 15 min “period” between the peaks of the brightenings. This “period” is similar to a ~ 10 min auroral spot brightening quasiperiod noted by Arballo et al. (1998) for the Jan 10, 1997 pseudobreakup event.

According to ground based observations (see Figure 3), the magnetic perturbations are weak, with ~ 140 nT and ~ 100 nT peak amplitudes, respectively. The magnetic bays are very localized with an area of $\sim 400 \text{ km} \times 1000 \text{ km}$. The time durations of these “minibays” are ~ 18 min and ~ 16 min. These signatures fit well with the characteristics of a pseudobreakup as described by McPherron (1991). The POLAR image date presented here

(see Plate 2) have shown that the auroral spot peak intensities are ~ 60 photons $\text{cm}^{-2} \text{s}^{-1}$ and ~ 50 photons $\text{cm}^{-2} \text{s}^{-1}$, localized to $\sim 3^\circ \times 6^\circ$ and $\sim 3^\circ \times 8^\circ$ areas with time scales of $\sim 10 - 15$ min. Thus we demonstrate for the first time that the auroral images are in excellent agreement with the ground based signatures in central location and both temporal and spatial scales. We believe that in the future UV images may be used as indicators of pseudobreakups (PBs) allowing researchers much better information on when and where such events occur and how much energy is involved in such events.

3.3 The Quiescent (non) event of June 13, 1998

Three out of 18 IP shock events have no obvious nightside auroral zone responses. One such event is shown in Figure 4 and Plate 3. In Figure 4, an IP shock is detected at 1920 UT by WIND instrumentation when WIND was at (145, 55, 25 R_E) GSM upstream of the Earth. Upstream of the IP shock, the magnetic field magnitude is stable and low (~ 5 nT). The IMF had a slight northward configuration (in GSM) with IMF $B_z \approx 1$ to 2 nT. The plasma density is low ($\sim 3 \text{ cm}^{-3}$) and the solar wind speed is also low (~ 315 km/s). The ram pressure is particularly low (less than 1 nPa). Across the shock, the magnetic field magnitude doubles and the IMF B_n increases to ~ 8 nT. The calculated ram pressure increases 3.5 times across the shock to ~ 3 nPa. The solar wind static pressure increases by 5 times and reached ~ 0.05 nPa.

The bottom panel of Figure 4 shows the AL (and AE) geomagnetic index. The vertical dashed line at ~ 2001 UT indicates the shock arrival time at the magnetopause. Prior to the shock arrival, AL is slightly positive (AE is less than ~ 60 nT, except for a small spike at ~ 1930 UT, a maximum of ~ 120 nT). After the IP shock arrival, AL decreases slightly to ~ -15 nT (and AE < 70 nT). There is no obvious auroral zone magnetic activity indicated in AL (or AE).

The UV images for an interval between the shock arrival and 25 min after the arrival are shown in the Plate 3. The calculated IP shock arrival time is at ~ 2001 UT (panel a). In the nightside auroral zone, there is no substorm or PB auroral activity. The quiescence midnight auroral zone denoted in Plate 3 is in agreement with the low AL and AE magnitudes. There is essentially no enhanced nightside auroral intensifications associated with the IP shock.

4. Statistical Results

All of the 18 events surveyed were classified into three different types of auroral activity. They are: 1) substorm expansion phase events, which are either freshly triggered (within 10 min of shock arrival) substorms or are further substorm intensifications of preexisting activity. Both types of activity appear as sudden auroral illumination increases. 2) Pseudobreakup (PB) events, which normally are small (less than $\sim 5^\circ$), localized near-midnight bright “spots” at auroral oval latitudes. 3) Quiescent events, which are cases where no significant auroral forms appeared in the near-midnight sector auroral zone within ~ 25 min after the IP shock arrival.

The interplanetary and magnetospheric preconditions of all 18 IP shock events are summarized in Table 2. In the first column, the types of auroral events are denoted as: SS or substorms, PB or pseudobreakups and QE or quiescent events. In the Table 2, the 8 solar wind parameters are: the IMF $|B|$, IMF B_s , IMF B_n and IMF B_z , the solar wind V_{sw} , N_p , P_{ram} and P_{st} . These parameters are calculated as 1.5 hr average upstream of the IP shock. The last column gives the magnetospheric 1.5 hr averages of AL prior to the IP shock arrivals.

In the Table 3, the changes in interplanetary parameters across the IP shocks are shown in the five columns next to the “Date” column. They are: the IMF B_z turnings, the downstream to upstream ratios of IMF $|B|$, V_{sw} , N_p , P_{ram} and P_{st} . The column labeled “Delay T” are the delay times between IP shock arrivals at the magnetopause and the onsets of near-midnight auroral activity. The time uncertainties are not included in the above Table. The delay times for substorm expansion phases are noted to be shorter than that for PB onsets. The delay times are ~ 4 to 10 min for substorm expansion, but ~ 12 to 20 min for PBs events. The center locations of auroral brightenings were also checked and the magnetic latitudes are listed in the column of “M Lat”. For substorm events, the auroral brightenings first occur at $\sim 65^\circ$ - 70° magnetic latitudes, while it is somewhat higher at $\sim 67^\circ$ - 72° for PB events. The column labeled “AL_{as} Peak” is the AL index maximum in the time interval between the shock arrival and shock arrival plus 30 min.

The 1.5 hr IMF B_z preconditions for all events are plotted graphically in Figure 5. For substorm events, the field is mainly southward prior to the IP shocks. For all PB and QE events, the IMF B_z preconditions are mainly zero or in a northward direction. A distinction between QEs and PBs can be shown by separating the IMF B_n and B_s components. This is shown in Figure 6. The IMF B_z preconditions for QE events is that there are no southward IMF components at all during the 1.5 hr upstream of the shock (and for even longer previous time, 2 - 3 hours). For PB events there are both southward and northward IMF components. In general, for PBs, the B_s values are lower than that for substorm events.

The ram pressure ratio increases (over the upstream pressures), give an indication of the shock strengths. As shown in the Table 3, this pressure ratio is not well correlated with the AL_{as} peak values (as other previous works had found). We note, however, that we do not have a large statistical sample. We did find that when the interplanetary preconditions

contain large IMF B_s and there are large ram pressure increases across the shock, the most intense substorms occurred. A typical example is the event on Sep 24, 1998. An explanation of this possible relationship will be shown later when we discuss a model for substorm triggering.

5. A Summary of the Observations

In this paper, we have organized our results by subdividing the nightside auroral activity into three different intensity levels. By doing so, we find that:

1) With southward IMF B_z preconditions, substorm expansion phase onsets (or substorm further intensifications) are triggered by IP shocks. This result is in good agreement with those of Burch (1972), Iijima (1973), Kokubun et al. (1977) and Brittnacher et al., (1999). It should be noted that in our study, 8 out of 18 events were substorm expansion phase events (44%), in excellent agreement with the 43% reported by Kokubun et al. (1977).

In our study, substorm onsets are identified by auroral UV images. By using images, it has been noted that IP shocks not only cause enhancements of preexisting localized substorm activity, but also initiate auroral precipitation at other local times as well. Use of AE indices cannot indicate such nuances.

2) With IMF $B_z \sim 0$ preconditions, PBs will occur. These are weak and localized auroral brightenings near midnight. PBs decay within ~ 10 min. PBs occurred in 7 out of 18 cases (39%), almost equal to the number of substorm cases. PBs can recur with ~ 10 to ~ 15 min quasiperiods.

3) With extreme northward IMF preconditions, i.e., $B_s = 0$ in the 1.5 hr (or longer) time intervals prior to IP shocks, there was no midnight auroral activity associated with IP shocks. This occurred in 3 out of the 18 events or 17% of the time.

4) Usually, the delay time for substorm expansion events is shorter than that for PB events. This is agreement with the Pulkkinen et al. (1998) observations and MHD simulation results.

Comments on PB observations

The longer delay times for PBs is consistent with the fact that the IMF preconditions for PBs is IMF $B_z \sim$ zero (while it is southward for SS events). During IMF $B_z \sim 0$ or B_n intervals, the auroral oval exists on higher magnetic latitudes (Meng and Makita, 1986; and Gary, et al., 1998). Higher L-shell magnetic fields map to further down tail distances. Thus, the longer delay times for PB events may simply be due to longer solar wind/tail and tail/ionosphere signal propagation/transport times.

It has been previously shown that, PBs have all the signatures of substorms except that they lack of global expansions (Sergeev et al., 1986; Koskinen et al., 1993; and Aikio et al., 1999). Our results are in agreement with this picture. Furthermore, we have shown that the factor which determines whether substorms or PBs occur is how much interplanetary energy is injected into the magnetotail ≤ 1.5 hr prior to shock arrival. If the interplanetary precursor energy (IMF B_s) is small, the magnetotail energy release is small (a PB results). If the precursor energy is large a substorm results. This conclusion is also consistent with PBs being small substorms (Davis and Hallinan, 1976; Koskinen et al., 1993). A similar conclusion was reached by Ohtani et al. (1993), inferred from a multisatellite study: PBs occur when “the energy stored in the magnetotail before the onset was not sufficient for the global development of a substorm”.

6. IP Shock Effects on the Magnetotail

6.1 The compression effects of IP shocks on the magnetotail

Below, we discuss the effects of solar wind compression of the near-Earth magnetotail.

Pressure balance between the solar wind and the tail geomagnetic field is assumed. The tail lobe geometry is primarily determined by the component of solar wind ram pressure normal to the tail boundary and secondarily, by solar wind static pressure. The equilibrium expression is:

$$\frac{B_L^2}{8\pi} = \rho_p V_{SW}^2 \sin^2 \alpha + nk(T_e + T_p) + \frac{B_{SW}^2}{8\pi} \quad (1)$$

Here B_L is the tail lobe magnetic field strength (we assume that the lobe plasma pressure is negligible), α is the tail flaring angle (the angle between the solar wind flow direction and the tangent to the magnetopause surface), T_e and T_p are the interplanetary electron and proton temperatures, and B_{SW} is the interplanetary field strength. The first term on the right-hand side is the component of the solar wind ram pressure perpendicular to the tail magnetopause. The second and third terms are the solar wind plasma thermal pressure and magnetic pressures. In this paper, we have called the sum of the latter two terms the “solar wind static pressure”.

Figure 7 shows the magnetopause positions in the X-Y GSM plane before and after the IP shock compression during the Sep 24, 1998 event discussed earlier. These are calculated based on the Petrinec and Russell (1996) model (which only considers the solar wind ram pressure). At $X = -15 R_e$ (down tail), the magnetopause radius is reduced from 19 to 13.7 R_e . By adding the static pressure we calculate that this radius is reduced further to 13.3 R_e . Assuming that magnetic flux in the tail lobes is conserved (no extra flux is added to or

reconnected in the tail), when the radius of the tail lobe is reduced from 19 to 13.3 R_e (at $X = -15 R_e$), the magnetic field in the lobes will increase by a factor of ~ 2.1 .

The magnetopause configuration and tail cross-section are sketched in Figure 8 (a) prior to and (b) after IP shock compression. As the lobe magnetic field strength is increased, the cross-tail current density will increase accordingly (as shown in Figure 8 b). The cross-tail current sheet is compressed, and if we assume that the compression is adiabatic, the current sheet thinning can be calculated assuming $(PV^\gamma)_{CS}$ is constant. Here P is the pressure in the current sheet, and V is the volume of the current sheet, and $\gamma = 5/3$. If one assumes that the cross-tail potential drop V_y remains constant during the compression, then the cross-tail electric field E_y will be enhanced as the tail diameter is decreased. We note that the stronger the IP shock (or resultant SSCs) are, the stronger the magnetotail compression. For the specific event of Sep 24, 1999, the variations in the tail at $X=-15 R_e$ are listed in Table 4.

Table 4. IP shock compression effect of Sep 24, 1998 event

<i>R:</i> 19 \Rightarrow 13.3 R_e		(at $X = -15 R_e$)
$B_L \Rightarrow 2.1 B_L$	$I \Rightarrow 2.1 I$ (mA /m)	
$P_L \Rightarrow 4.4 P_L$	$h \Rightarrow h/1.7$	$(PV^\gamma)_{CS} = const.$
$V_y \Rightarrow const.$	$E_y \Rightarrow 1.43 E_y$	

6.2 Current sheet Disruption

Magnetotail current sheet disruption (Lui et al., 1988) has been proposed for the initiation of the expansion phase of a magnetospheric substorm. In this model, the near-earth portion of the cross-tail current is drastically reduced or disrupted. Part of the cross-tail current flows along the magnetic field lines to the ionosphere, across the ionosphere and returns to

the plasma sheet along the magnetic fields. A current wedge is thus formed. Coroniti (1985) has proposed the tearing instability, Papadopoulos (1979) the lower hybrid drift instability (LHDI), and Lui, et al. (1990) the kinetic cross-field streaming instability (KCSI) as the microinstability that lead to the current sheet disruption.

As proposed by Lui et al. (1990), the KCSI can set in when the drift speed between electrons and ions are sufficiently large such that electron Landau damping is overcome by the ion contribution to growth. One possible way to increase the relative drift between electrons and ions is by increasing cross-tail electric field E_y , discussed earlier. Clearly, other instabilities can also be triggered by the enhanced currents as well.

We use the ion Weibel instability as one example to illustrate the effects of IP shock compression. The growth rate γ of the unstable waves is (Chang et al., 1990):

$$\gamma = \omega_{pi} V_0 / C \quad (3)$$

where ω_{pi} is the ion plasma frequency, V_0 is the ion drift speed along the E_y direction. The larger the E_y is, the greater the V_0 will be when ions become unmagnetized. For a low plasma sheet density of 0.5 cm^{-3} , the current sheet disruption can occur when $V_0 > 600$ km/s (with a growth rate of $\gamma > 0.3$, A.T. Lui, private communication, 1999). For high plasma sheet densities with $N_i = 6 \text{ cm}^{-3}$, the instability will occur when $V_0 > 180$ km/s.

The above numbers imply that when the plasma sheet density is tenuous, the drift speeds need to be higher to cause instability. According to this Weibel instability scenario, one may explain the observations of substorm, PB and QE triggering at IP shocks presented in this paper. During northward IMF preconditions, little or no flux transfer to the tail occurs,

thus the plasma sheet will be of low density. For these conditions, shock compression will be insufficient to cause the Weibel instability to go, and thus, there will be no substorm expansion phase. On the other hand, for southward IMF preconditions, the plasma sheet will be “primed” and then moderate compression of the tail will trigger the Weibel instability, and current sheet disruption and substorm onset will follow. For only moderate priming, IP shock compression may or may not lead to energy release from the plasma sheet. These minimal energy release events are PBs.

The reader should note that the substorm triggering dependence on the strength of the IP shock is explained by this model quite well. With a stronger interplanetary shock and southward IMF precondition, the microinstability threshold will be lowered even further, and thus tail current sheet disruption will occur more easily.

7. A Dripping, Tilting Bucket Model

We have shown that by considering the interplanetary “preconditions”, the IMF B_z component prior to IP shock arrival, the magnetospheric responses to the 18 IP shocks can be nicely ordered. We have used a magnetotail current disruption mechanism initiated by a Weibel instability, to illustrate how different interplanetary preconditions can lead to substorm expansive phases, pseudobreakups and quiescent events.

In this study, the Weibel instability has been used as the “microinstability” mechanism leading to current disruption. Clearly other instabilities could be operative as well. In the near future, we will be examining several other microinstabilities analytically to determine which ones would be most easily triggered by IP shock compression and which ones might be most likely to be operative in the tail leading to substorm expansion phases.

To illustrate the findings in this paper and our conceptual ideas, a schematic is provided in Figure 9. On the left hand side of the figure, solar wind energy is put into the plasma sheet by dayside magnetic reconnection (the small pail putting water into the bucket). The greatest rate of energy input occurs when the IMF has a long duration and large southward component (top left panel), less so when $B_z \approx 0$ (middle left panel), and the least, when the IMF has a completely northward component (bottom left panel).

The top left panel shows a scenario similar to the “leaky bucket” substorm model where energy flows out of the bucket from a spigot. However, one additional feature of our model is that the energy in the bucket (energy stored in the tail) also continuously “drips” out. This “dripping” is greatest when the energy storage is large (top panel) and least when it is slight (bottom panel). This interpretation implies that the energy output into the magnetosphere/ionosphere (the flow from the spigot) is less than that which is being put in (the small pail).

This “dripping” is implied from the limited ~ 1.5 hr priming found in this study and many other previous works, such as Arnoldy (1971), Tsurutani and Meng (1972) and Meng et al. (1973) and many others. If the energy was stored in the plasma sheet for much longer time intervals, the relationship found here and the previously cited works showing high IMF B_z -AE correlations would not be present. What exactly are these loss processes? At this time we don’t exactly know. But several possibilities are internal dissipation and down tail energy flow. Ho and Tsurutani (1997) have argued that deep tail magnetic reconnection is not related to substorm activity, so this “magnetotail sloughing” may be one possible dissipation mechanism.

A prime feature of this model is that there is no real magnetospheric “ground state”. The “dripping” asymptotically slows down as the tail energy decreases, and a ground state will only be reached at time infinity.

On the right hand side of Figure 9 are the IP shock effects. The shock “tilts” bucket. The stronger the shock, the greater the tilting. In the top right panel, the shock (bucket tilting) leads to substorm “intensification”. At this time, more energy is pouring out from the spigot (there is more energy going into the ionosphere than the solar wind is transferring to the plasma sheet).

For the case where the plasma sheet energy storage level is relatively low (middle right panel), a moderate shock leads only to a pseudobreakup (small substorm). A stronger shock corresponds to greater bucket tilting, and a substorm. For very low energy storage (bottom right panel), a moderate shock leads to no energy output. However, for a very strong shock, a PB or even a substorm are possible outcomes.

In the above model, the IMF B_z (dayside magnetic reconnection) plays the role of filling of the bucket. The shock compression and cross-tail current sheet microinstability is schematically represented by the tilting of the bucket. The “dripping, tilting bucket” model clearly predicts certain shock/magnetosphere/ionosphere relationships. Various facets of this model are testable which we hope to do using the upcoming solar maximum WIND/ACE and POLAR data.

Akasofu and Chao (1980) have shown evidence of IP shock triggering of substorms when the shock is accompanied by IMF B_z southward turnings. From this evidence they argued for a “directly driven” response of the magnetosphere/magnetotail system. There is some evidence for such a mechanism in the events studied here. Five of the eight substorm

events had southward IMF turnings at the shock. Thus, it is possible that a directly driven mechanism is also operative for these events. However, for the totality of our study, our storage-release mechanism can explain all of the data reasonably well.

8. Final Comments

We want to leave the reader with a sense of the usefulness of studying shock-triggered substorms to understand substorm processes. Shock compressions are typically very large perturbations of the magnetosphere/magnetotail system, much larger than northward or southward turnings of the interplanetary magnetic fields. Because of the strength of these “perturbations”, magnetospheric responses should be predictable and measurable. A second advantage of studying shock triggered events is that shock dimension along the earth-sun line are very small (shocks are discontinuities which pass the spacecraft within seconds) and have very large spatial scales in the other two directions. The typical scales of the latter are fractions of an AU, much larger than the size of the magnetosphere. Thus a fast-forward (or fast-reverse) shock detected at IMP 8, WIND or ACE can be assumed to compress (or decompress) the entire magnetosphere with an appropriate propagation time delay. On the other hand, IMF B_s or B_n events are typically parts of interplanetary Alfvén waves which often have scale sizes smaller than $60 R_e$ (Tsurutani et al, 1995). Thus B_s or B_n (Alfvénic) turnings are often only coherent over only part of the magnetosphere, leading to ambiguous interpretations of the results.

That shocks are thin discontinuities and cause dayside auroral brightenings are facts that can be put to great advantage in other types of future studies. The first auroral brightenings could potentially give very accurate timings of the IP shock compressions of the magnetosphere (within seconds, if a more rapid imaging cadence could be acquired). The delay time of the onset of substorms or PBs with an accurate measure of the down tail

shock velocity (within 1%), gives one an excellent handle on where in the tail the “action” is taking place. The only missing pieces of the puzzle are the times for instability/reconnection development, and the time for propagation of the signal from the tail to the ionosphere. If the down tail location becomes better defined through these techniques, one could search the tail for specific plasma wave modes/bursty bulk flows to experimentally identify the specific microscopic triggering mechanism(s).

Acknowledgment. Portions of this paper represent work done at the Jet Propulsion Laboratory, California Institute of Technology, Pasadena, under contract with the National Aeronautics and Space Administration. We thank C.T. Russell and A.T.Y. Lui for the helpful scientific discussions. T. Araki provided the ground based AL and AE indices, G. Rostoker and T. Hughes CANOPUS magnetometer data and K. Ogilvie and R.P. Lepping the WIND SWE and MFI data. J.K. Arballo helped in the data processing and software support. X.-Y. Zhou would like to thank the National Research Council for the award of a Resident Associateship at the Jet Propulsion Laboratory.

References

- Aikio, A.T., V.A. Sergeev, M.A. Shukhtina, L.I. Vagina, V. Angelopoulos, and G.D. Reeves., Characteristics of pseudobreakups and substorms observed in the ionosphere, at the geosynchronous orbit, and in the midtail, *J. Geophys. Res.*, 104, 12263, 1999.
- Akasofu, S.-I., and J.K. Chao, Interplanetary shock waves and magnetospheric substorms, *Planet. Space Sci.*, 28, 381, 1980.
- Arballo, J.K., C.M. Ho, G.S. Lakhina, B.T. Tsurutani, X.-Y. Zhou, Y. Kamide, J.-H. Shue, S.-I. Akasofu. R.P. Lepping, A.S. Sharma, C.C. Goodrich, K. Papadopoulos

- and J.G. Lyon, Pseudobreakups during January 10, 1997, *International Conference on Substorms-4*, ed. Y. Kamide and S. Kokubun, pp.315-318, Terra Sci., Tokyo, 1998.
- Arnoldy, R.L., Signature in the interplanetary medium for substorms, *J. Geophys. Res.*, **76**, 5189, 1971.
- Brittnacher, M., M. Wilber, M. Fillingim, D. Chua, G. Parks, J. Spann, and G. Germany, Global auroral response to a solar wind pressure pulse, *Advanced in Space Research*, in press, COSPAR'98, 1999.
- Burch, J.L., Preconditions for the triggering of polar magnetic substorms by storm sudden commencements, *J. Geophys. Res.*, **77**, 5629, 1972.
- Chang, C.L., H.K. Wong, and C.S. Wu, Electromagnetic instabilities attributed to a cross-field ion drift, *Phys. Rev. Lett.*, **65**, 1104, 1990.
- Coroniti, F.V., Explosive tail reconnection: the growth and expansion phases of magnetospheric substorms, *J. Geophys. Res.*, **90**, 7427, 1985.
- Davis, T.N., and T.J. Hallinan, Auroral spirals, 1, Observations, *J. Geophys. Res.*, **81**, 3953, 1976.
- Gary, J.G., L.J. Zanetti, B.J. Anderson, T.A. Potemra, J.H. Clemmons, J.D. Winningham, and J.R. Sharber, Identification of auroral oval boundaries from in situ magnetic field measurements, *J. Geophys. Res.*, **103**, 4187, 1998.
- Heppner, J.P., Note on the occurrence of world-wide ssc's during the onset of negative bays at College, Alaska, *J. Geophys. Res.*, **60**, 29, 1955.
- Ho, C. M., and B.T. Tsurutani, Distant tail behavior during high speed solar wind streams and magnetic storms, *J. Geophys. Res.*, **102**, 14165, 1997.
- Iijima, T., Interplanetary and ground magnetic conditions preceding ssc-triggered substorms, *Rep. Ionos. Space Res. Jap.*, **27**, 205, 1973.
- Kawasaki, K., S.-I. Akasofu, F. Yasuhara, and C.-I. Meng, Storm sudden commencements and polar magnetic substorms, *J. Geophys. Res.*, **76**, 6781, 1971.

- Kokubun, S., R.L. McPherron, and C.T. Russell, Triggering of substorms by solar wind discontinuities, *J. Geophys. Res.*, *82*, 74, 1977.
- Koskinen, H.E.J., R.E. Lopez, R.J. Pellinen, T.I. Pulkkinen, D.N. Baker, and T. Bosinger, Pseudobreakup and substorm growth phase in the ionosphere and magnetosphere, *J. Geophys. Res.*, *98*, 5801, 1993.
- Lepping, R.P., M.H., Acuna, L.F. Burlaga, W.M. Faffell, J.A. Slavin, K.H. Schatten, F. Mariani, N.F. Ness, F.M. Neubauer, Y.C. Whang, J.B. Byrnes, R.S. Kennon, P.V. Panetta, J. Scheiffle, and E.M. Worley, The WIND magnetic field investigation, in *The Global Geospace Mission*, ed. by C.T. Russell, Kluwer, 207, 1995.
- Lui, A.T.Y., et al., A case study of magnetotail current sheet disruption and diversion, *Geophys. Res. Lett.*, *15*, 721, 1988.
- Lui, A.T.Y., A. Mankofsky, C.-I. Chang, K. Papadopoulos, and C.S. Wu, A current disruption mechanism in the neutral sheet: a possible trigger for substorm expansions, *Geophys. Res. Lett.*, *17*, 745, 1990.
- McPherron, R.L., Physical processes producing magnetospheric substorms and magnetic storms, in *Geomagnetism*, vol., edited by J.A. Jacobs, p. 593, Academic, San Diego, Calif., 1991.
- Meng, C.-I., B. Tsurutani, K. Kawasaki, and S.-I. Akasofu, Cross-correlation analysis of the AE index and the interplanetary magnetic field Bz component, *J. Geophys. Res.*, *78*, 617, 1973.
- Meng, C.-I, and K. Makita, dynamic variation of the polar cap, in *Solar Wind-Magnetospheric Coupling*, edited by Y. Kamide and J.A. Slavin, pp. 605, Terra Sci., Tokyo, 1986.
- Ogilvie, K.W., D.J. Chornay, R.J. Fritzeneriter, F. Hunsaker, J. Keller, J. Lobell, G. Miller, J.D. Scudder, E.C. Sittler, Jr., R.B. Torbert, D. Bodet, G. Needell, A.J. Lazarus, J.T. Steinberg, J.H. Tappan, A. Mavertic, and E. Gergin, SWE, A

- comprehensive plasma instrument for the WIND spacecraft, in *The Global Geospace Mission*, ed. by C.T. Russell, Kluwer, 55, 1995.
- Ohtani, S. B.J. Anderson, D.G. Sibeck, P.T. Newell, L.J. Zanetti, T.A. Potemar, K. Takahashi, R.E. Lopez, V. Angelopoulos, R. Nakamura, D.M. Klumpar, and C.T. Russell, A Multisatellite study of a pseudo-substorm onset in the near-Earth magnetotail, *J. Geophys. Res.*, 98, 19355, 1993.
- Papadopoulos, K., The role of microturbulence on Collisionless Reconnection, in *Dynamics of the Magnetosphere*, ed. by S.-I. Akasofu, p.289, 1979.
- Petrinec, S.M., and C.T. Russell, Near-Earth magnetotail shape and size as determined from the magnetopause flaring angle, *J. Geophys. Res.*, 101, 137, 1996.
- Pulkkinen, T.I., D.N. Baker, M. Wiltberger, C. Goddich, R.E. Lopez, and J.G. Lyon, Pseudobreakup and substorm onset: Observations and MHD simulations compared, *J. Geophys. Res.*, 103, 14847, 1998.
- Schildge, J.P., and G.L. Siscoe, A correlation of the occurrence of simultaneous sudden magnetospheric compressions and geomagnetic onsets with selected geophysical indices, *J. Atmos. Terr. Phys.*, 32, 1819, 1970.
- Sergeev, V.A., A.G. Yahnin, R.A. Rakhmatulin, S.I. Solovije, F.S. Mozer, D.J. Williams, and C.T. Russell, Permanent flare activity in the magnetosphere during periods of low magnetic activity in the auroral zone, *Planet. Space Sci.*, 34, 1169, 1986.
- Torr, M.R., D.G. Torr, M. Zukic, R.B. Johnson, J. Ajello, P. Banks, K. Clark, K. Cole, C. Keffer, G. Parks, B. Tsurutani, and J. Spann, A far ultraviolet imager for the international solar-terrestrial physics mission, *Space Sci. Rev.*, 71, 329, 1995.
- Tsurutani, B.T., and C.-I. Meng, Interplanetary magnetic-field variations and substorm activity, *J. Geophys. Res.*, 77, 2964, 1972.

- Tsurutani, B.T., W.D. Gonzalez, A.L.C. Gonzalez, F. Tang, J.K. Arballo, and M. Okada, Interplanetary origin of geomagnetic activity in the declining phase of the solar cycle, *J. Geophys. Res.*, *100*, 21717, 1995.
- Tsurutani, B.T., X.-Y. Zhou, J.K. Arballo, W.D. Gonzalez, G.S. Lakhina, V. Vasyliunas, J.S. Pickett, T. Araki, H. Yang, G. Rostoker, T.J. Hughes, R.P. Lepping, and D. Berdichevsky, Auroral zone dayside precipitation during magnetic storm initial phases, submitted to *J. Atmos. Solar-Terr. Phys.*, 1999.
- Winterhalter, D., E.J. Smith, M.E. Burton, N. Murphy, and D.J. McComas, The heliospheric plasma sheet, *J. Geophys. Res.*, *99*, 6667, 1994.
- Zhou, X.-Y., and B.T. Tsurutani, Rapid intensification and propagation of the dayside aurora: Large scale interplanetary pressure pulses (fast shocks), *Geophys. Res. Lett.*, *26*, 1097, 1999.

Figure Captions

Figure 1. Interplanetary magnetic field and solar wind plasma measured by WIND at (183, 13, -9 Re) GSM during the September 24, 1998 event. The vertical line in the upper solar wind parameter panel indicates the IP shock at 2320 UT. The vertical line in the bottom AE and AL panels shows the IP shock arrival time at the magnetopause at 2345 UT.

Plate 1. Dayside and night auroral activity during the Sep 24 1998 IP shock event. A magnetic coordinate system is used with local noon on the top and dawn on the right hand side. The center of each image is the north magnetic pole. The time sequence is from (a) to (i). The IP shock arrives at the Earth's magnetopause between panel (b) and (c) with a significant dayside auroral brightening intensification at (c). The IP shock associated substorm auroral further intensification appears in panel (f) (2348:25 UT) with a illumination of over $120 \text{ photons cm}^{-2} \text{ s}^{-1}$ near 21 MLT.

Figure 2. The interplanetary magnetic field and solar wind plasma measured by WIND at (112, -55, 4 Re) GSM during the August 9, 1997 event. The upper vertical line at 0610 UT indicates the front ramp of the pressure pulse. The vertical line in the bottom panel indicates the time of 0644 UT when the pressure pulse arrives at the Earth.

Figure 3. A map (panel a) and X-component stack plot of CANOPUS magnetometers on August 9, 1997. Panel (b) is the ground meridian chain. Panel (c) is the ground longitudinal chain. In panels (b) and (c), the vertical solid line (at ~ 0655 UT) shows the PB onset from ground measurements. GILL is at (56° , 265°) geographic latitude and longitude, RABB at (58° , 256°), FSMI at (60° , 248°), FCHU at (59° , 266°) and ISLL at (54° , 265°).

Plate 2. The pseudobreakup on August 9, 1997. The images were taken using the LBH short filter (~140-160 nm) with a ~ 37 sec exposure time. A geographic coordinate system is used with local noon near the top left of the image and midnight near the bottom right. Time evolves from panel (a) to (o). Panel (f) shows the PB onset ~ 12 min after the shock arrival (panel b).

Figure 4. Interplanetary magnetic field and solar wind plasma measured by WIND at (145, 54, 26 Re) GSM during the June 13, 1998 event. In the top panel, the vertical line indicates the IP shock. The vertical dashed line in the lower panel is the time of the IP shock arrival at Earth (2001 UT).

Plate 3. The nightside auroral activity after IP shock arrival at Earth. A geomagnetic coordinate system is used, with local midnight at the bottom. The estimated IP shock arrival time is 2001 UT, panel (a).

Figure 5. The IMF B_z “preconditions” for substorm, PB and QE events. The bars indicate the 1.5 hr average of IMF B_z upstream of IP shocks. Event date are in chronological order for each type of geomagnetic event.

Figure 6. The IMF preconditions and the magnetospheric responses for the 18 events. The top panel is for 1.5 hr average B_n (defined in the text) upstream of the IP shocks. The middle is 1.5 hr average B_s (defined in the text) upstream of the IP shocks. The peak AL index after the IP shock arrival at Earth is shown in the bottom panel.

Figure 7. The tail magnetopause position ($X \leq 0$) during the Sep 24, 1998 event. At $X = -15 R_e$ in the tail, the radius of the magnetopause is decreased from $19 R_e$ to $13.7 R_e$ by the solar wind ram pressure.

Figure 8. The magnetopause and magnetotail configurations prior to and after IP shock compression. The increases in tail current densities and magnetic fields are indicated by thicker lines and larger symbols for the magnetic field directions.

Figure 9. A schematic of the Dripping, Tilting Bucket model.

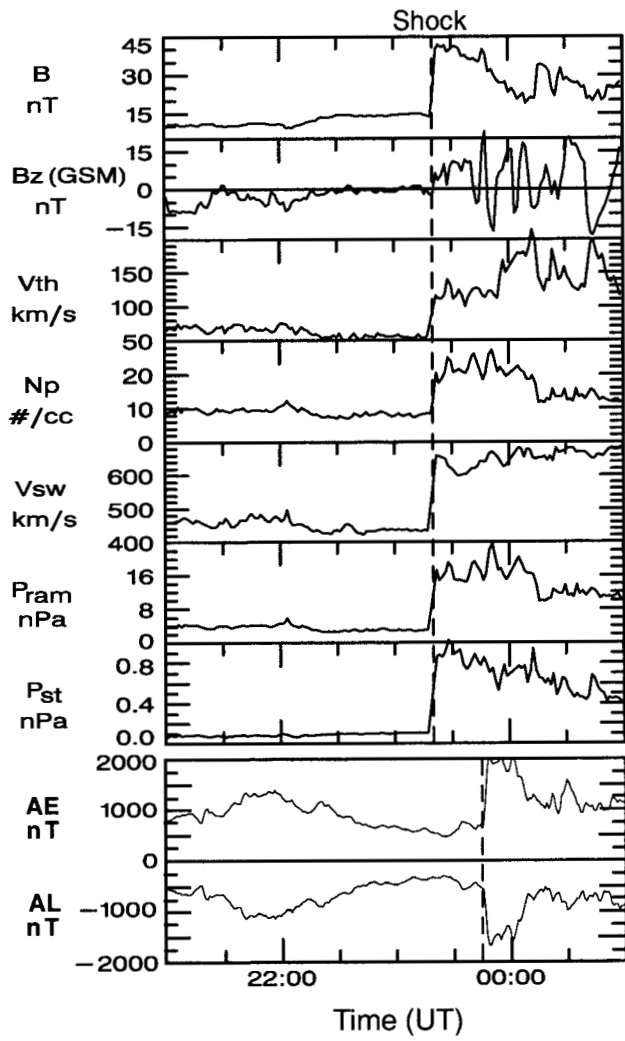


Figure 1.

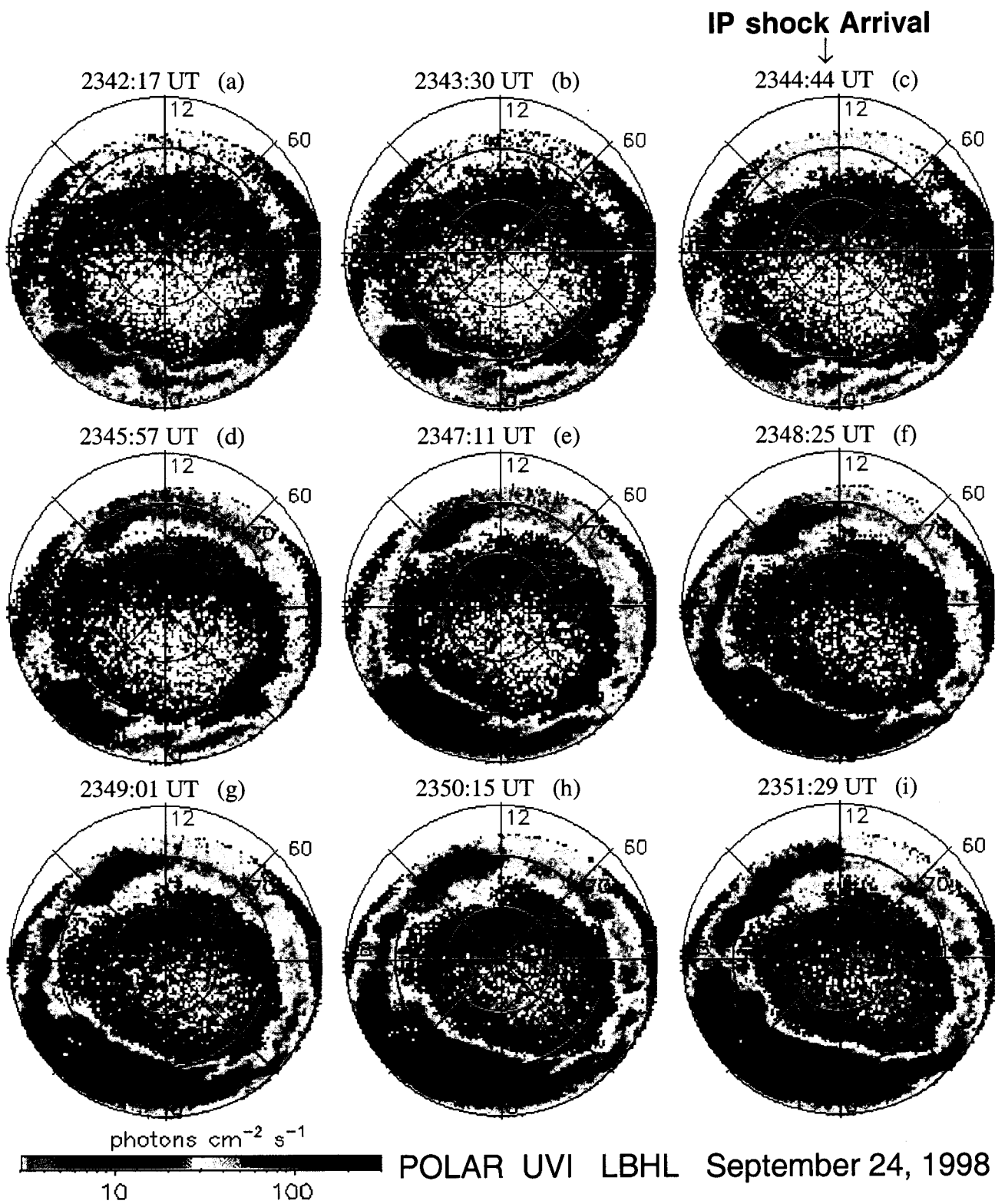


Plate 1.

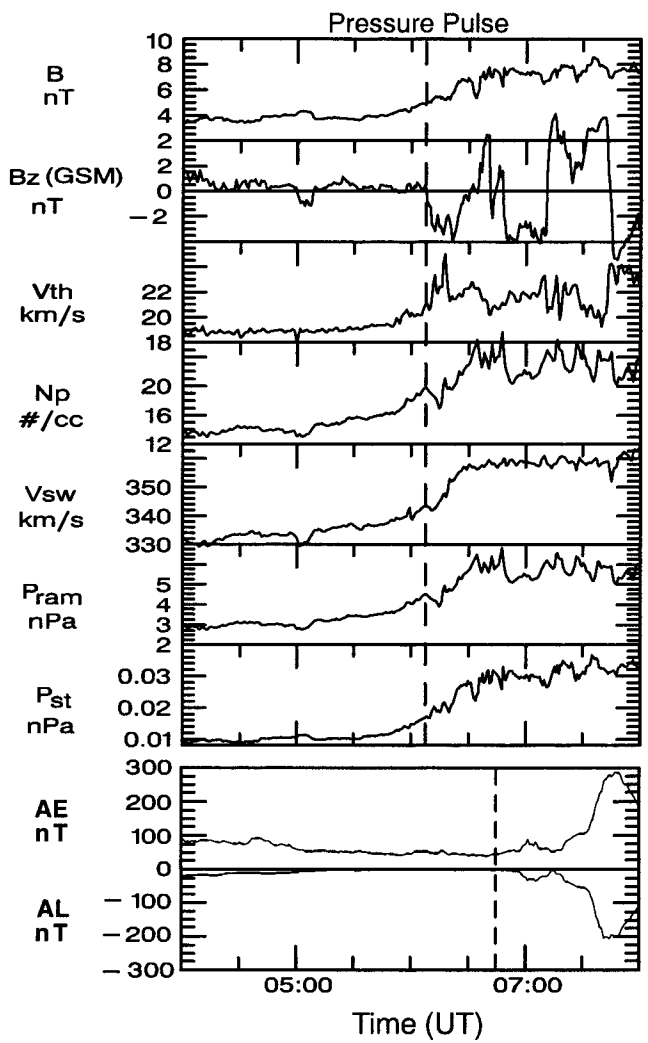


Figure 2

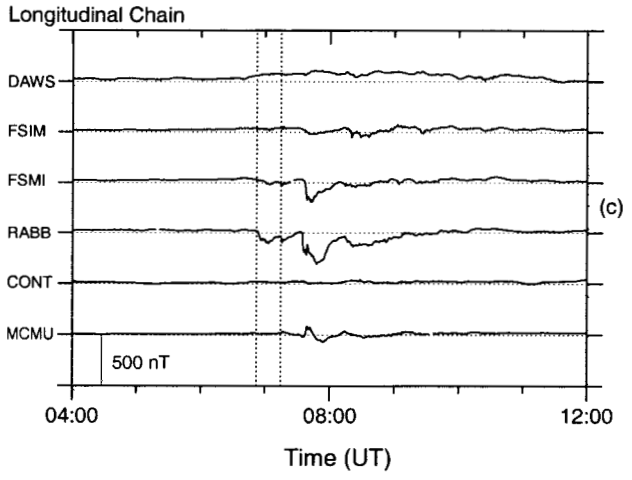
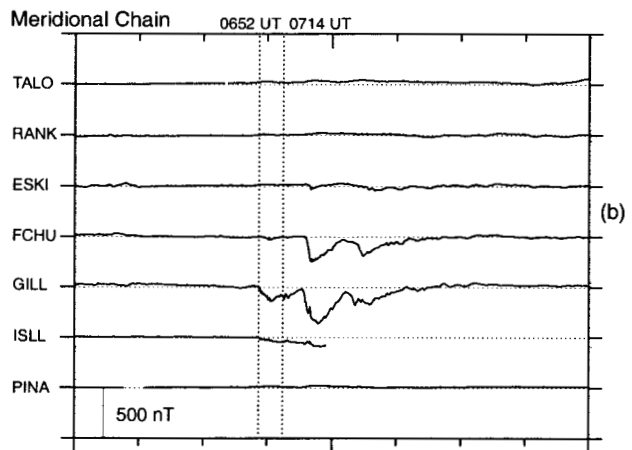
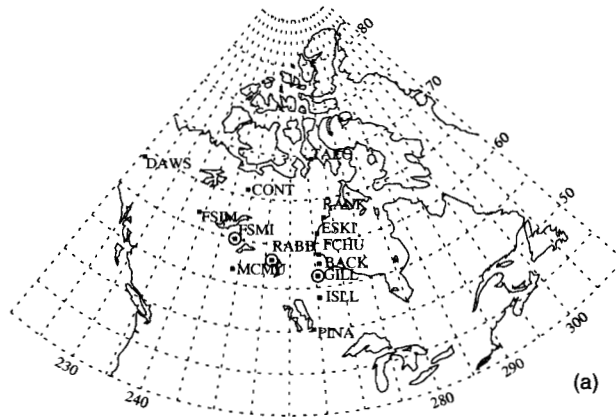


Figure 3

Pressure Pulse Arrival

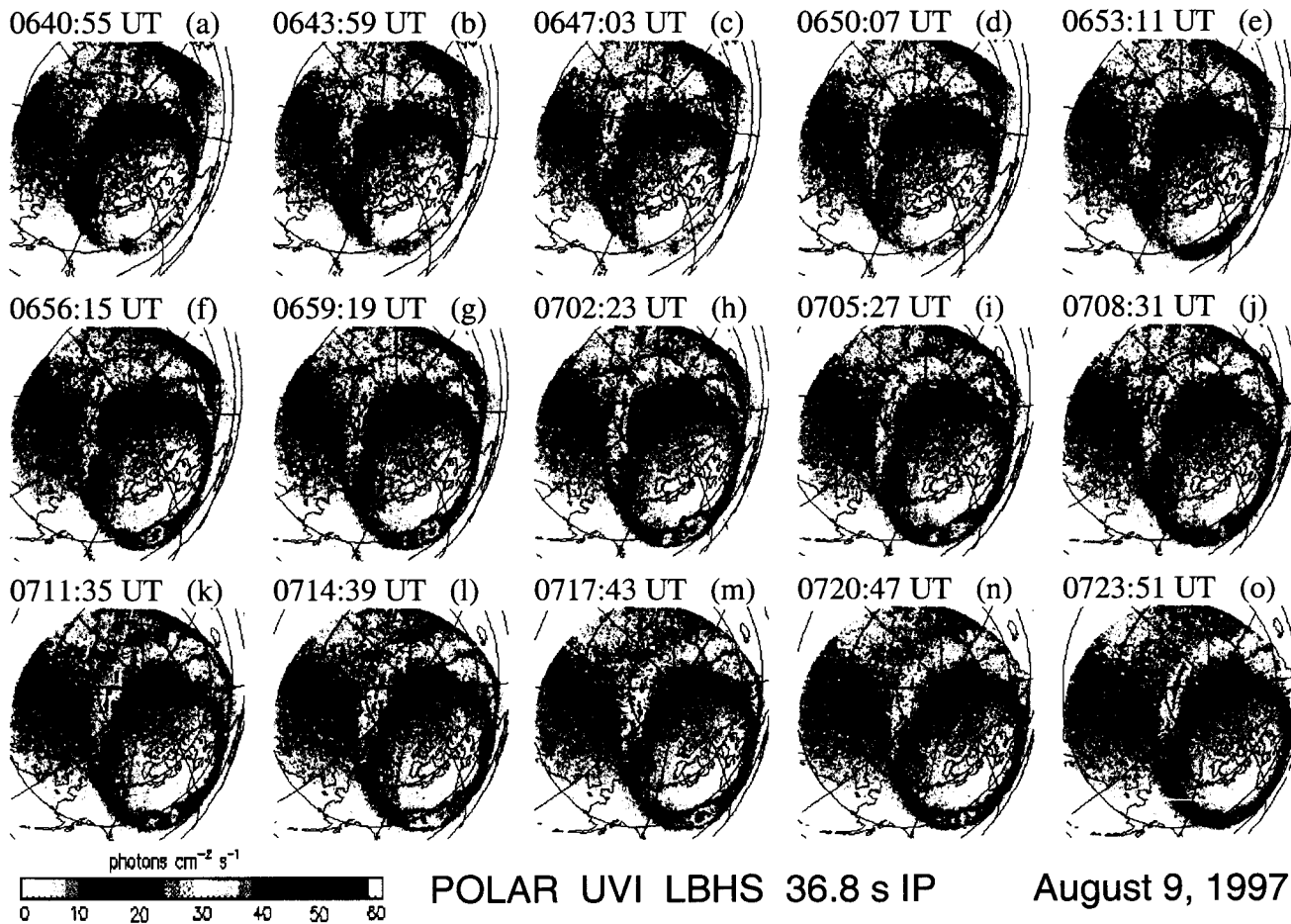


Plate 2.

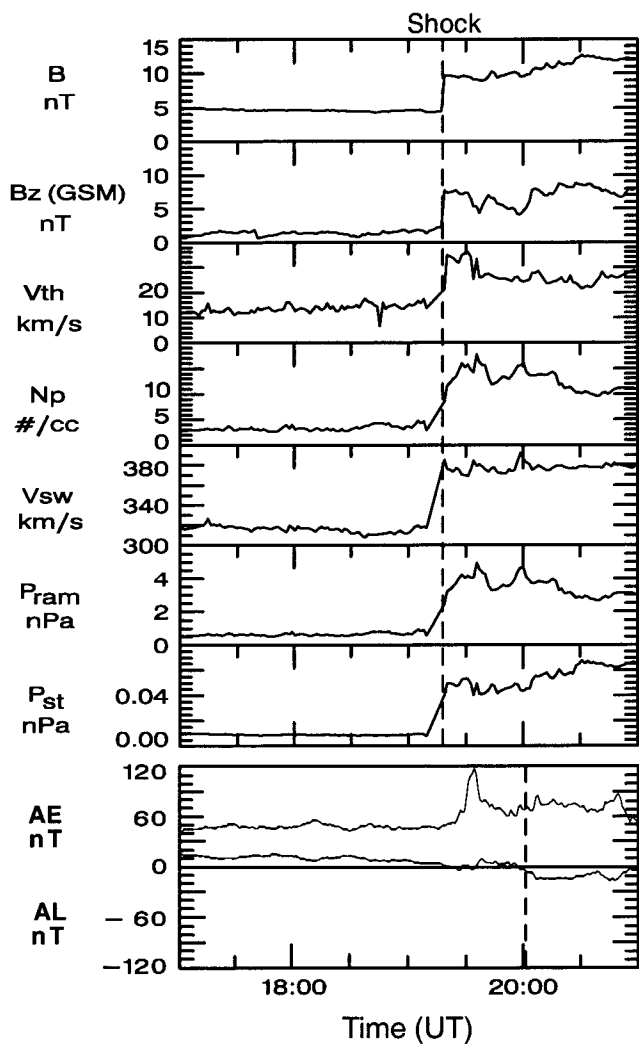


Figure 4

IP shock Arrival

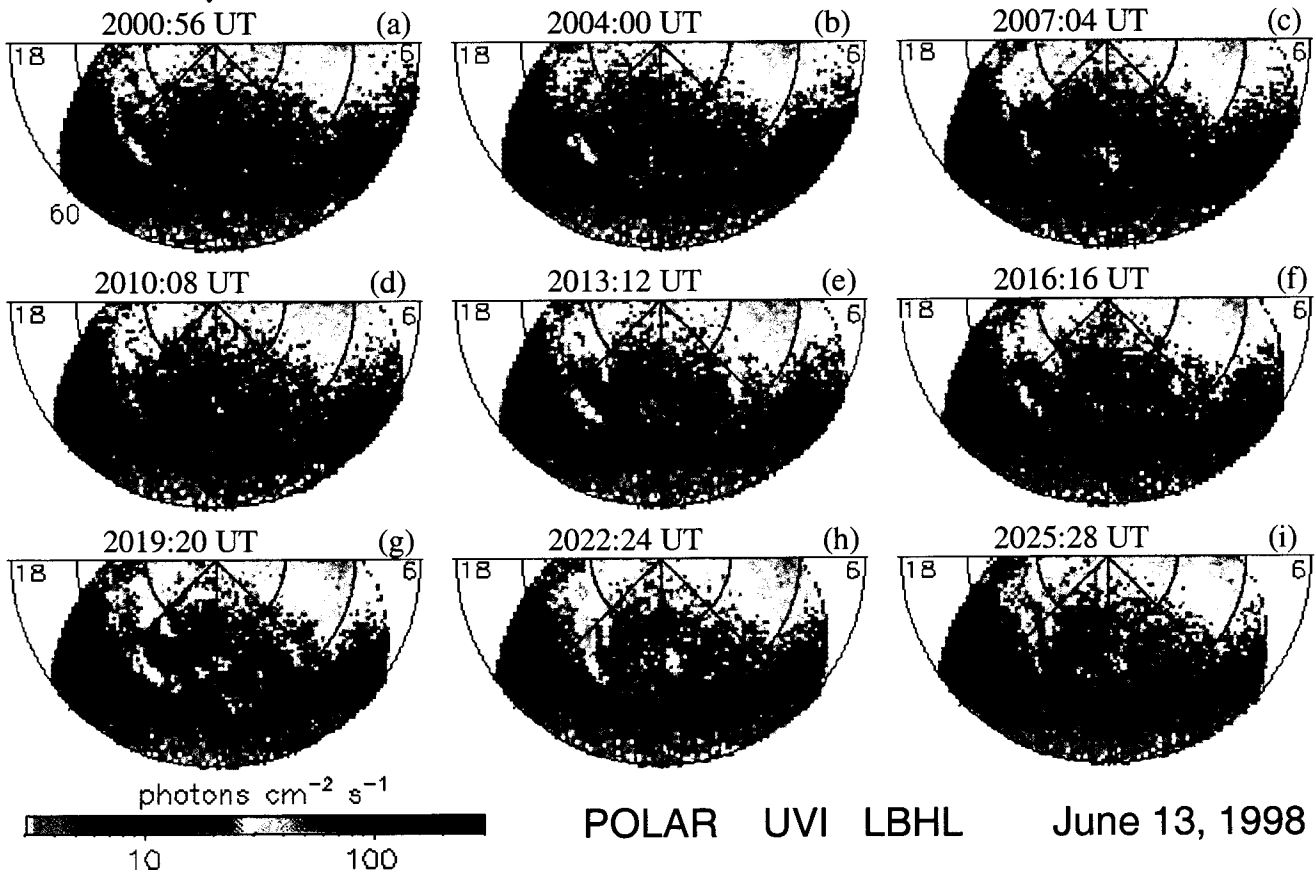


Plate 3.

Table 2. Preconditions of 18 IP shock associated events

Type	Date	IMF \bar{B} (nT)	IMF \bar{B}_s (nT)	IMF \bar{B}_n (nT)	IMF \bar{B}_z (nT)	\bar{V}_{sw} (km/s)	\bar{N}_p (#/cc)	\bar{P}_{ram} (nPa)	\bar{P}_{st} (nPa $\times 10^{-3}$)	$\bar{A}L_{ps}$ (nT)
SS	Sep 18, 1997	6.7	6.4	0.0	-6.4	331	12.2	3.5	20.3	-302
	Oct 1, 1997	3.5	1.5	0.9	-0.05	429	12.6	4.1	11.4	-68
	Oct 10, 1997	8.9	1.6	1.8	-0.03	414	11.8	4.5	34.6	-43
	Nov 22, 1997	6.4	2.3	1.3	-0.7	349	12.6	3.4	32.7	-37
	Apr 7, 1998	7.1	1.2	0.0	-1.2	293	10.4	2.0	23.0	-35
	May 3, 1998	3.2	1.4	0.0	-1.4	430	4.7	2.0	4.6	-32
	May 29, 1998	11.3	4.2	1.9	-1.7	518	8.8	5.3	90.4	-165
	Sep 24, 1998	12.3	2.7	0.7	-1.8	446	8.6	3.9	94.8	-498
	Jan 10, 1997	2.4	0.1	0.4	0.3	375	7.7	2.4	5.5	-5
Aug 9, 1997	3.9	0.5	0.4	0.3	335	15.0	3.8	10.8	0	
Oct 23, 1997	5.0	0.3	1.4	1.3	300	7.5	1.5	14.9	-8	
PB	Nov 1, 1997	6.0	1.6	1.1	0.1	341	30.7	8.0	21.9	-42
	Dec 10, 1997	6.2	1.1	2.4	2.0	286	11.0	2.0	19.6	-5
	Sep 8, 1998	9.0	1.5	1.0	0.2	328	4.7	1.1	33.0	-61
	Oct 2, 1998	6.6	0.4	1.3	0.6	511	3.7	2.2	25.9	-22
QE	Jun 13, 1998	4.6	0.0	1.4	1.4	315	3.4	0.8	9.0	3
	Jun 25, 1998	11.1	0.0	10.0	10.0	400	14.1	5.1	51.4	9
	Aug 10, 1998	4.9	0.0	0.7	0.7	400	4.8	1.7	11.0	-89

Table 3. Solar wind parameter variations at IP shocks and geomagnetic responses

Type	Date	IMF Bz (nT) Turning	IMF($\Delta B/\bar{B}$)	$(\Delta V/\bar{V})_{sw}$	$(\Delta N_p/\bar{N}_p)$	$(\Delta P/\bar{P})_{ram}$	$(\Delta P/\bar{P})_{st}$	Delay T (min)	M Lat ($^{\circ}$)	$A L_{as}$ Peak (nT)
SS	Sep 18, 1997	-6 to -9	0.4	0.07	0.4	0.4	0.9	6	66	-491
	Oct 1, 1997	-2 to 5	2.8	0.08	2.3	2.3	3.9	9	67	-185
	Oct 10, 1997	-0.5	0.6	0.07	0.7	0.7	1.4	10	65	-190
	Nov 22, 1997	0 to -5	1.4	0.29	1.7	3.1	7.3	6	65	-363
	Apr 7, 1998	-1 to -7	0.8	0.14	1.4	1.6	2.4	6	70	-263
	May 3, 1998	-2 to -6	1.3	0.15	1.2	3.2	5.1	9	65	-136
	May 29, 1998	6 to -10	0.7	0.26	9.5	1.8	2.5	5	69	-955
	Sep 24, 1998	-1 to 3	2.3	0.48	1.4	4.1	9.7	4	65	-1670
	Jan 10, 1997	1 to 4	1.6	0.11	1.0	1.4	5.5	19	70	-24
	Aug 9, 1997	1 to -6	0.7	0.07	0.4	0.4	0.9	12	67	-35
PB	Oct 23, 1997	4 to 7	1.3	0.13	0.3	0.6	2.0	13	71	-9
	Nov 1, 1997	2 to 5	0.6	0.04	0.5	0.6	1.1	12	71	-22
	Dec 10, 1997	-1 to -3	1.7	0.26	1.6	2.4	6.0	12	72	-4
	Sep 8, 1998	1 to -2	0.2	0.12	2.8	0.9	0.6	12-13	68	-111
	Oct 2, 1998	5 to -2	1.8	0.40	1.8	3.3	9.9	6	70	-299
QE	Jun 13, 1998	2 to 8	1.1	0.19	8.6	3.5	4.7	N/A	N/A	-15
	Jun 25, 1998	9 to 13	0.6	0.09	0.1	0.6	1.3	N/A	N/A	-9
	Aug 10, 1998	1 to -1	1.1	0.12	9.4	1.6	3.3	N/A	N/A	-123

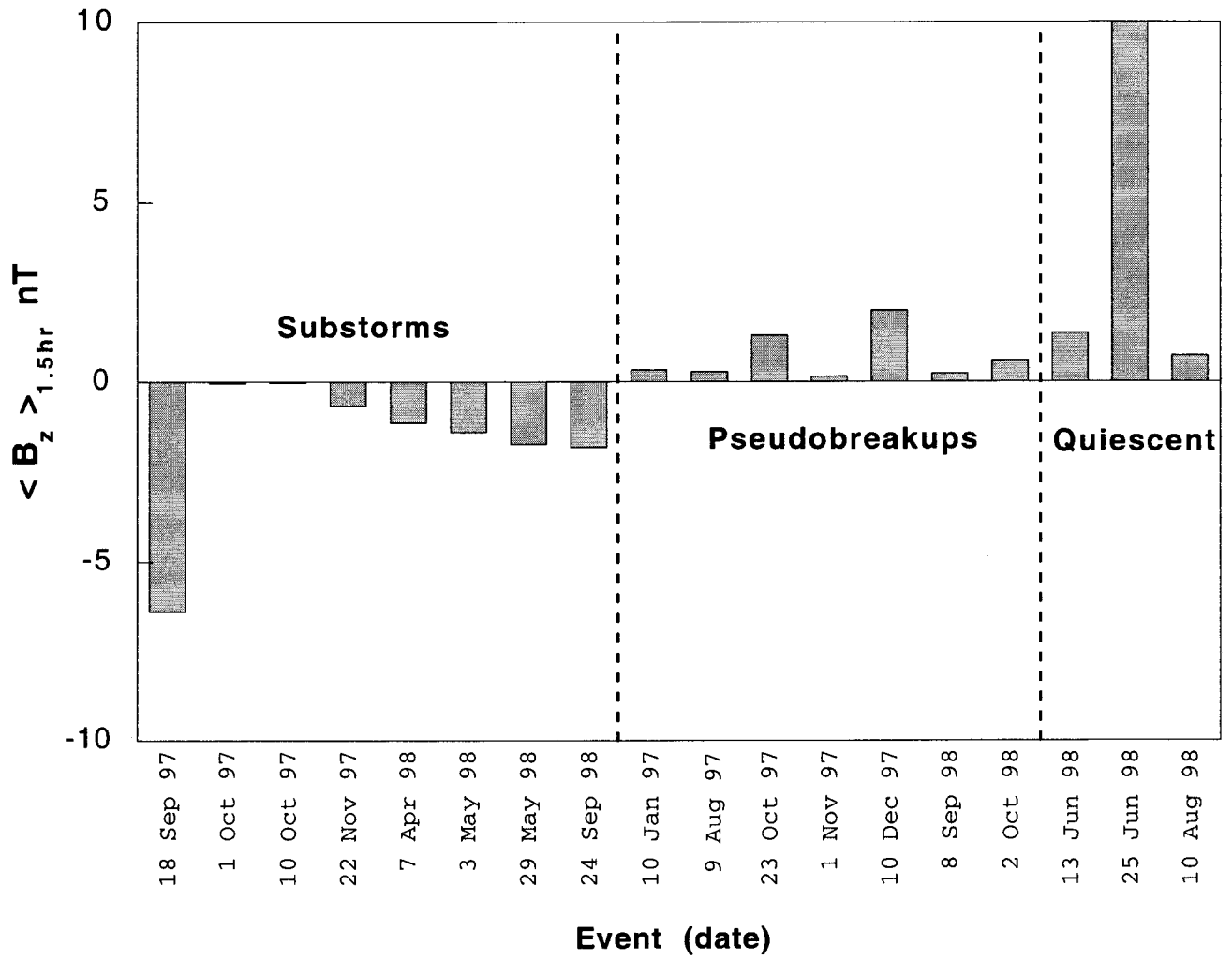


Figure 5

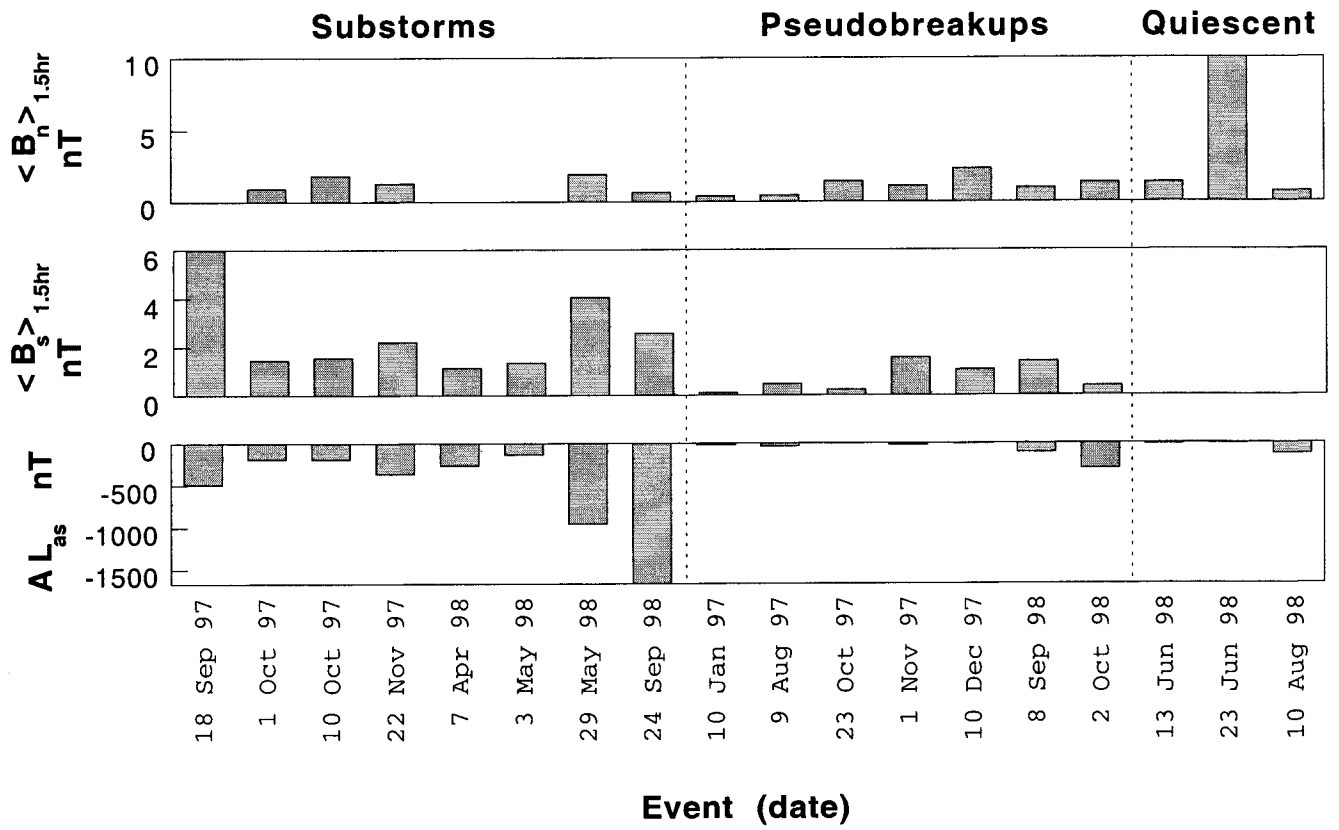


Figure 6

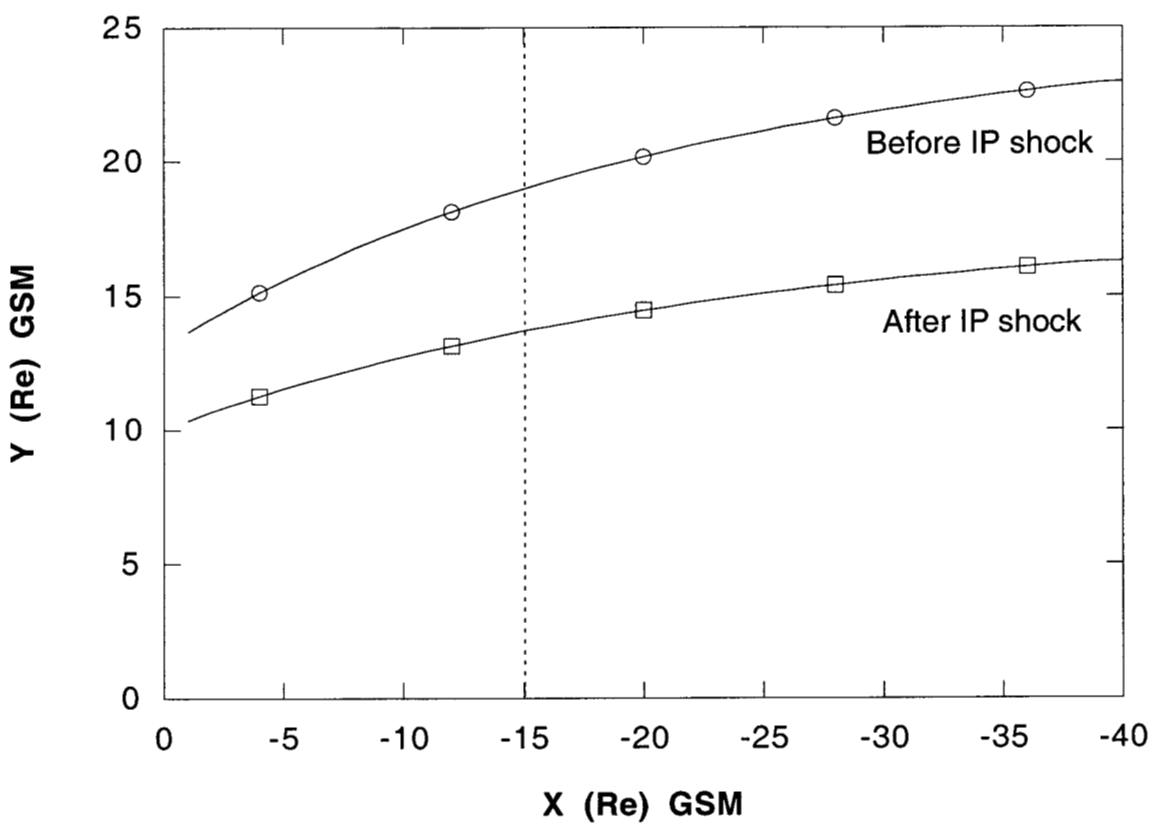
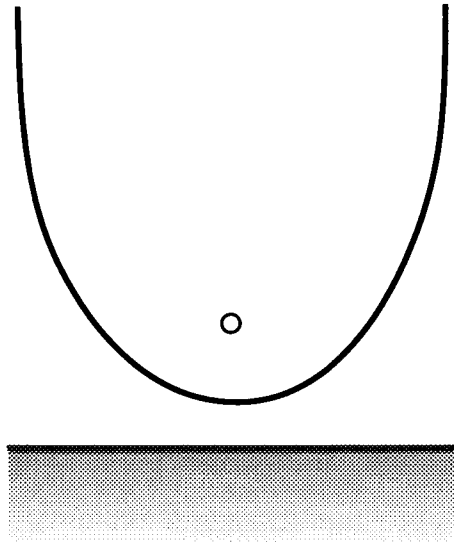
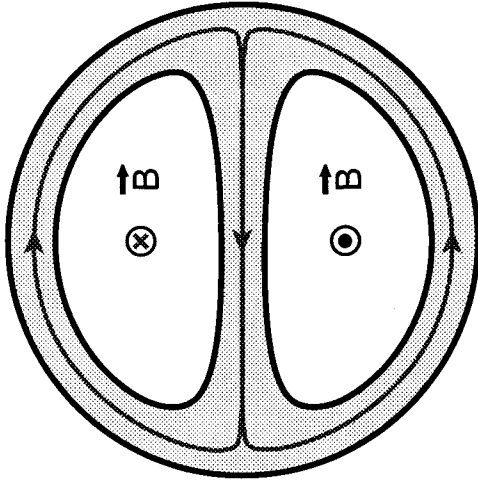


Figure 7

Shock front

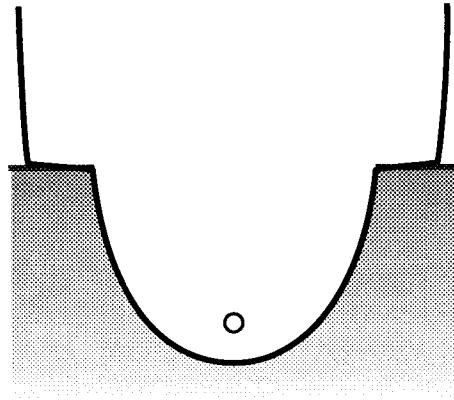


Magnetotail



(a)

Shock front



(b)

Figure 8

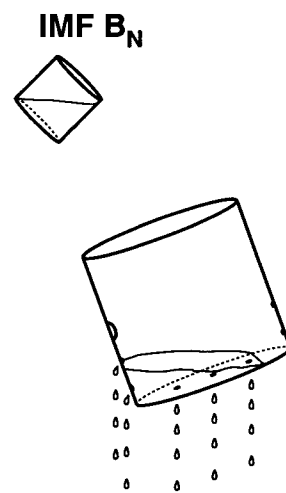
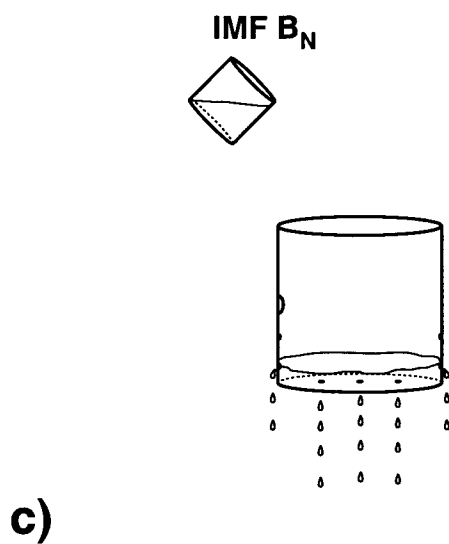
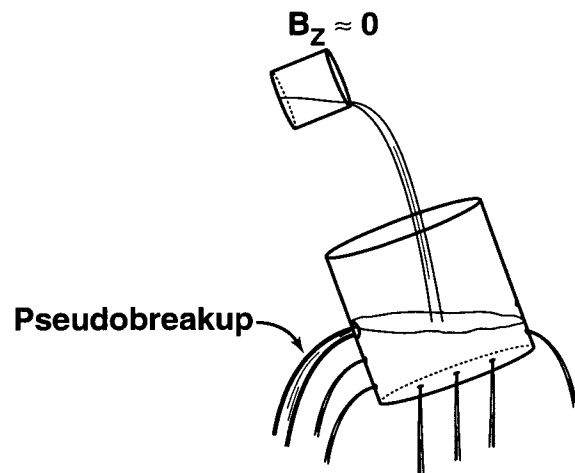
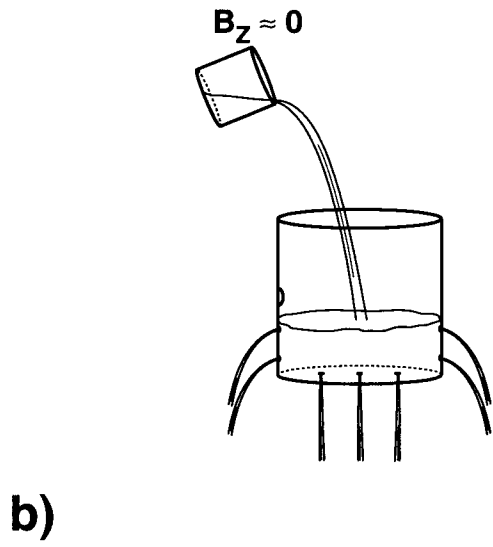
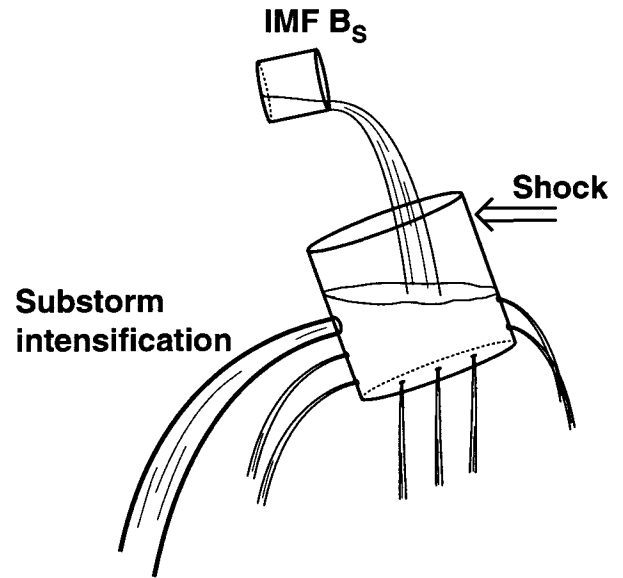
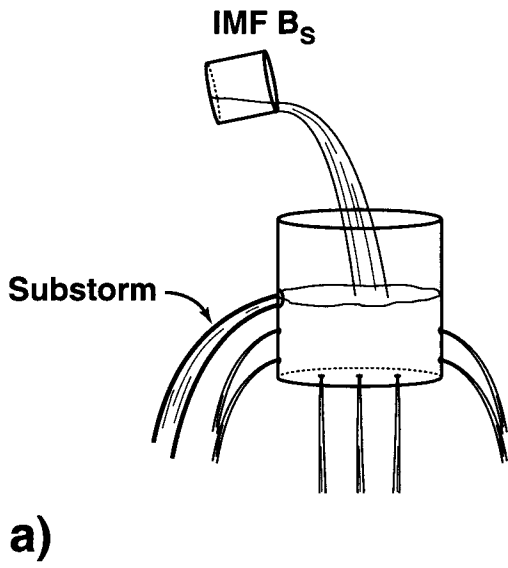


Figure 9